Similar but not the same: methods and applications of quantitative MRI to study muscular dystrophies

Veeger, T.T.J.

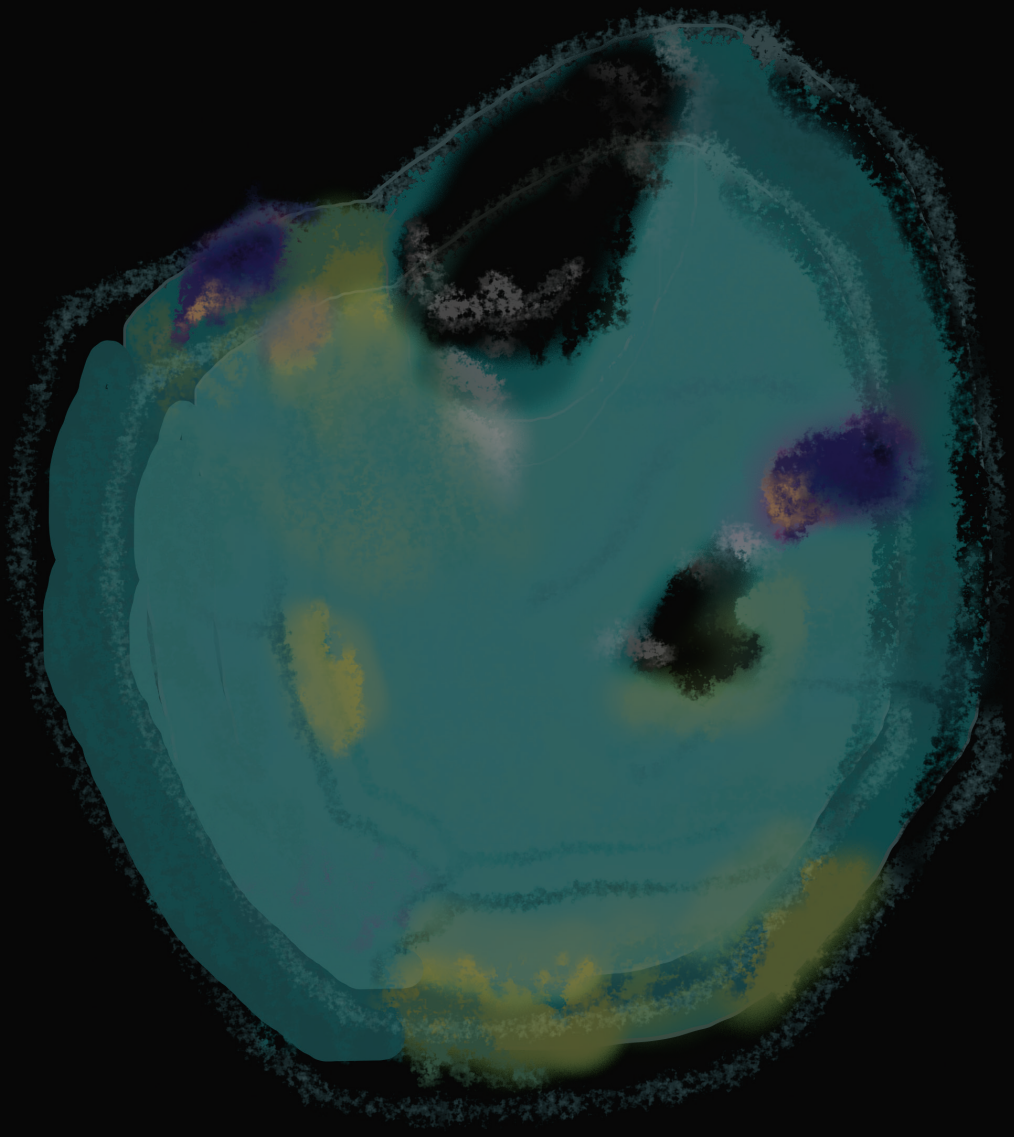

CHAPTER 2

MUSCLE ARCHITECTURE IS ASSOCIATED WITH MUSCLE FAT REPLACEMENT IN DUCHENNE AND BECKER MUSCULAR DYSTROPHIES

Thom T.J. Veeger MSc[1]
Erik W. van Zwet PhD[2]
Diaa al Mohamad PhD[2]
Karin J. Naarding MD[3]
Nienke M. van de Velde MD[3]
Melissa T. Hooijmans PhD[4]
Andrew G. Webb PhD[1]
Erik H. Niks MD PhD[3]
Jurriaan H. de Groot PhD[5]
Hermien E. Kan PhD[1]

Muscle and Nerve: August 2021 – Volume 64 – Issue 5 - 10.1002/mus.27399

[1] C.J. Gorter MRI Center, Department of Radiology, Leiden University Medical Center, Leiden, The Netherlands
[2] Department of Biostatistics, LUMC, Leiden, Netherlands
[3] Department of Neurology, LUMC, Leiden, Netherlands
[4] Department of Radiology & Nuclear Medicine, Amsterdam University Medical Centers, Location AMC
[5] Department of Rehabilitation medicine, LUMC, Leiden, Netherlands

ABSTRACT

Introduction/Aims

Duchenne and Becker muscular dystrophies (DMD and BMD, respectively) are characterized by fat replacement of different skeletal muscles in a specific temporal order. Given the structural role of dystrophin in skeletal muscle mechanics, muscle architecture could be important in the progressive pathophysiology of muscle degeneration. Therefore, the aim of this study was to assess the role of muscle architecture in the progression of fat replacement in DMD and BMD.

Methods

We assessed the association between literature-based leg muscle architec-tural characteristics and muscle fat fraction from 22 DMD and 24 BMD patients. Dixon-based magnetic resonance imaging estimates of fat fractions at baseline and 12 (only DMD) and 24 months were related to fiber length and physiological cross-sectional area (PCSA) using age-controlled linear mixed modeling.

Results

DMD and BMD muscles with long fibers and BMD muscles with large PCSAs were associated with increased fat fraction. The effect of fiber length was stronger in muscles with larger PCSA.

Discussion

Muscle architecture may explain the pathophysiology of muscle degeneration in dystrophinopathies, in which proximal muscles with a larger mass (fiber length x PCSA) are more susceptible, confirming the clinical observation of a temporal proximal-to-distal progression. These results give more insight into the mechanical role in the pathophysiology of muscular dystrophies. Ultimately, this new information can be used to help support the selection of current and the development of future therapies.

INTRODUCTION

Duchenne and Becker muscular dystrophies (DMD and BMD, respectively) are X-linked recessive diseases caused by mutations in the *DMD* gene leading to the absence (in DMD) or dysfunction (in BMD) of the dystrophin protein. The diseases are characterized by progressive muscle weakness associated with a gradual increase in the volume fraction of fat in muscle, and the presence of muscle inflammation and fibrosis[1]. The progression of fat replacement in different muscles exhibits a typical temporal order[2,3] where, in general, the proximal muscles degenerate before the distal ones[4]. The pathophysiology of the muscle degeneration in DMD and BMD is poorly understood and it is also unknown why specific muscles are more susceptible to degeneration than others. The identification of factors that affect muscle preservation could support the selection of current and the development of future therapies.

Dystrophin is a vital part of the costamere, which connects the muscle fiber to the sarcolemma, providing mechanical stability within the muscle fiber[5–7]. The role of the costamere is to protect the contractile element from damage during dynamic contractions[5–7] and to shunt the contractile forces from the contractile filaments to the sarcolemma, resulting in fast force propagation over the muscle fiber[8].

The spatial distribution of sarcomeres over the muscle determines the dynamic properties of the muscle. The number of serial-organized sarcomeres defines the muscle fiber length and potential contraction velocity, whereas the number of parallel-organized sarcomeres determines the muscle physiological cross-sectional area (PCSA) and the maximum muscle force[9]. Given the differences in muscle architecture and the structural role of dystrophin in the mechanics of the muscle fiber, muscle architecture may be an important property in the temporal order of fat replacement. Muscles with long fibers may be more susceptible to damage because of a higher inhomogeneity of instantaneous force distribution within the muscle fibers during activation[10]. Muscles with a larger PCSA could be more susceptible to damage because the load on muscle fibers can be higher during vigorous contractions. At submaximal loading, however, a large PCSA may be protective against damage because of relatively low fiber stresses, as the same force is divided over a larger area.

Magnetic resonance imaging (MRI) is ideally suited to assess the temporal order of muscle fat replacement in muscle disease. Several quantitative MRI studies in DMD and BMD have yielded important information about which muscles in the leg are susceptible to fat replacement early in the disease, and which muscles are relatively spared[2,11–15]. In DMD, this order has been associated with the amount

of eccentric contraction during walking[16]. However, the correlation was only present when excluding two muscles from the analysis. The authors applied simple linear regression analyses and a cross-sectional design and therefore could not correct for the effect of age. A major disadvantage of simple linear regression analyses in a progressive disease such as a muscular dystrophy is that because fat fraction (FF) increases with age, any variable correlating with age correlates with FF as well[17].

In this study we aimed to study the association between the increase in FF in DMD and BMD over time and fiber length and PCSA, while controlling for the effect of age. We hypothesize that fiber length and PCSA are associated with FF.

METHODS

MRI data acquisition

The DMD MRI data set used in this study was described by Hooijmans et al. and Naarding et al.[17,18] and the BMD data set by Hooijmans et al.[19]. In short, male DMD and BMD patients were scanned at baseline and after about 1 (only DMD) and 2 years. All patients were recruited from the Dutch Dystrophinopathy Database and diagnosis was confirmed by genetic testing[20]. Our study was approved by the local medical ethics committee. Written informed consent was given by all patients and/or their parents.

MRI acquisition and analysis

MRI examinations were performed on a 3T MR scanner (Ingenia, Philips Healthcare, Best, The Netherlands) and included a 3-point gradient-echo Dixon sequence (23 slices; voxel size: 1 x 1 x 10 mm; slice gap: 5 mm; repetition time [TR]/echo time [TE]/echo time shift [ΔTE]: 210/4.41/0.76 ms; 2 averages; flip angle [FA]: 8°) to assess muscle fat replacement in the upper and lower leg muscles. The scans were aligned perpendicular to the femur and tibia.

Water and fat images were reconstructed offline using the same in-house water-fat separation algorithm as Hooijmans et al.[19], built in Matlab 2019b (MathWorks, Natick, Massachusetts MA, USA). This algorithm was based on the known frequencies of a six-peak lipid spectrum[21].

The images were visually checked for bulk motion artefacts and were excluded if these were present. Regions of interest (ROIs) were drawn in five slices for ten upper and seven lower leg muscles using the program Medical Image Processing, Analysis and Visualization (MIPAV) (http://mipav.cit.nih.gov). The most proximal slice with the biceps femoris short head still visible was chosen to be the center

of the five upper leg slices; the thickest part of the calf was chosen to be the center for the five lower leg slices. The ten upper leg muscles consisted of the rectus femoris (RF), vastus medialis (VM), vastus lateralis (VL), vastus intermedius (VI), biceps femoris long head (BFL), semitendinosus (ST), semimembranosus (SM), adductor magnus (AM), gracilis (GR) and sartorius (SAR). The seven lower leg muscles were the gastrocnemius medialis (GM), gastrocnemius lateralis (GL), soleus (SOL), tibialis anterior (TA), tibialis posterior (TP), extensor digitorum longus (EDL) and peroneus (PER). Fat replacement was quantified by the fat fraction per muscle (*FF*) and per slice *i* using the signal intensity of fat (SI_{FAT}) from the fat image and water (SI_{WATER}) from the separate water image (Eq.1)

$$FF(i) = \frac{SI_{FAT}(i)}{SI_{FAT}(i) + SI_{WATER}(i)} \quad \text{Eq.1}$$

Subsequently, a weighted average of the five slices was calculated per muscle (Eq. 2)

$$FF = \frac{\Sigma(FF(i) * N_P(i))}{\sum N_P(i)} \text{ for } i = [1-5] \text{ slices} \quad \text{Eq. 2}$$

where $N_p(i)$ is the total number of pixels of the muscle ROI per slice.

Muscle characteristics

The PCSA and muscle fiber lengths (L_f) of adult muscles were extracted from the data reported by Ward et al.[22]. The reported PCSAs contain an additional cosine factor to be able to relate PCSA to force (Eq. 3), and do not represent the actual PCSAs describing surface of parallel sarcomeres and estimated by muscle volume over fiber length[23].

$$\frac{muscle\ mass\ [g] * \cos(\theta\ [^\circ])}{fibre\ length\ [cm] * \rho\ [g/cm^3]} \quad \text{Eq. 3}$$

The θ is the pennation angle and ρ is the muscle density of 1.056 g/cm^3. Therefore, we derived the "classical" PCSA by dividing the PCSA values of Ward et al.[22] by the cosine of the pennation angles, reported in same study, and included the classical values in our analyses.

Table 1. Descriptive statistics

		DMD	BMD
Patients	Count	22	24
Age [years]	Mean (SD)	9.9 (3.0)	41.4 (12.8)
	Range	6.5 – 17.4	18.8 – 68.2
Height [cm]	Mean (SD)	137.1* (20.9)	179.1* (7.6)
Weight [kg]	Mean (SD)	45.3* (22.2)	77.0* (12.4)
Lost ambulation			
Baseline	Count	9	0
12 months	Count	10	-
24 months	Count	10	1
Fat fraction			
Upper leg	Mean (SD)	0.453 (0.260)	0.441 (0.310)
Lower leg	Mean (SD)	0.310 (0.210)	0.245 (0.206)

*DMD = Duchenne muscular dystrophy; BMD = Becker muscular dystrophy; SD = standard deviation; * = not available for all patients*

Statistical analysis

For every patient we acquired data from two or three time-points and multiple muscles. A linear mixed-effects model was used to analyze the relation between muscle characteristics and muscle fat replacement. The model and graphs were built using R software (R Core Team, 2019) in combination with the packages *lme4*[24] and *visreg*[25]. The full code is made publicly available at Github (https://git.lumc.nl/neuroscience/2021-veegerttj-lmem-in-dmd-bmd; using version at commit 4924b94c).

The *FF* is limited between 0 and 1 and thus not normally distributed. In addition, the age-dependent *FF* follows an S-shaped "logistic growth" curve rather than a linear relationship[17,26]. To obtain a normal distribution and a linear relationship between *FF* and age, a logit transformation of the *FF* data (*logFF*) was applied:

$$logFF = \ln\left(\frac{FF}{1 - FF}\right) \qquad \text{Eq. 4}$$

The linear mixed-effects model design also included mean-centered variables *age* [year], L_f [cm] and *PCSA* [cm^2], and an interaction term (L_f *x PCSA*) for each of the 17 leg muscles as predictor (fixed) variables. To account for varying disease progression and onset between patients and muscles, random effects were included according to the design with the highest Log-Likelihood value, being a by-patient and by-muscle random intercept and slope for the effect of *age*.

P-values were obtained by t tests using the *lmerTest* package[27] and significance was set at $p < .05$. Holm-Bonferroni correction was applied to adjust for multiple comparisons (ie, for each of the four fixed effects)[28].

RESULTS

For three DMD patients, no usable upper leg MRI scans were acquired at any of the three timepoints, either due to image artefacts or because the patient could not complete the scan (Figure 1). In total, 39 MRI scans were available for the upper leg, and 44 for the lower leg, over all three time-points (see Table 1 for descriptive statistics and Supplemental Table 1 and 2 for an overview of mutations). For BMD, all data were included and, in total, 43 MRI scans were available for both upper and lower leg over the two time-points (Figure 1).

The median *FF* of individual muscles for all DMD and BMD patients at baseline (Figure 2) showed that the AM and BFL had the highest *FFs*, AM highest in DMD and BFL in BMD, and that the EDL and TP had the lowest *FFs*.

An association between *age* and *logFF* was observed in DMD and BMD (Table 2), with a higher *age* corresponding to a higher *logFF* (positive slope). L_f was also associated with *logFF* for both DMD and BMD, showing that muscles with longer fibers were associated with a higher *logFF*. By contrast, *PCSA* was significantly associated with *logFF* only in BMD patients. The interaction L_f x PCSA was significantly associated with *logFF* in both DMD and BMD, where the effect of L_f on *logFF* was stronger if *PCSA* was larger. The association between *age* and *logFF* was stronger in DMD than BMD, whereas the other three associations L_f, *PCSA* and L_f*x PCSA*, were stronger in BMD than DMD patients.

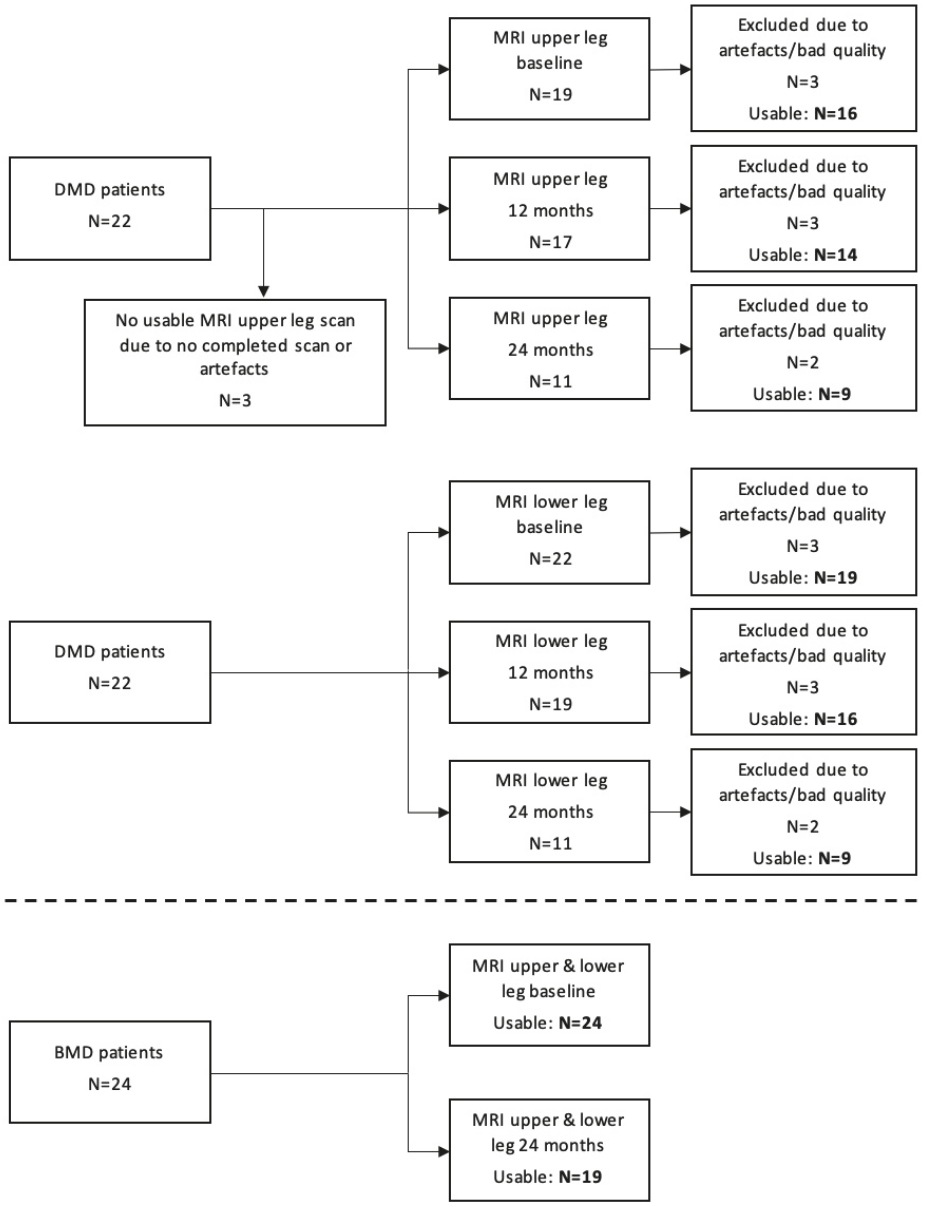

Figure 1: Details on the inclusion of DMD and BMD patients and longitudinal upper and lower leg MRI scans. For DMD, in total 39 usable data sets were available for the upper leg and 44 for the lower leg. For BMD, 43 usable datasets were available for the upper and lower leg. Abbreviations: BMD, Becker muscular dystrophy; DMD, Duchenne muscular dystrophy; MRI, magnetic resonance imaging

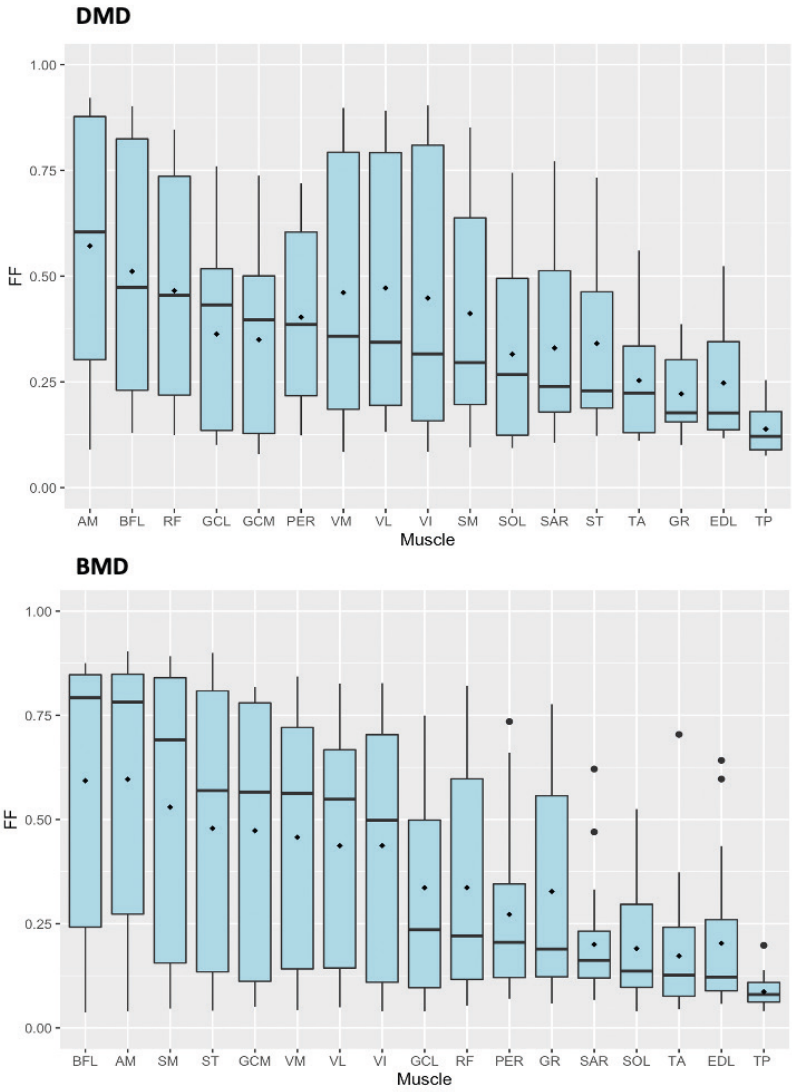

Figure 2: FF per muscle over all DMD (upper panel) and BMD (lower panel) patients for the baseline measurement. Lines within boxes indicate the median value and define the order on the x axis, black diamonds represent the mean, and the lower and upper bounds indicate the first and third quartiles. Upper whiskers show the largest value with, as maximum, 1.5 x IQR, and lower whiskers show the smallest value with, as minimum, 1.5 x IQR. Individual round dots represent outliers. Muscles are ordered from highest median FF on the left to lowest median FF on the right. Abbreviations: AM, adductor magnus; BFL, biceps femoris long head; BMD, Becker muscular dystrophy; DMD, Duchenne muscular dystrophy; EDL, extensor digitorum longus; FF, fat fraction; GL, gastrocnemius lateralis; GM, gastrocnemius medialis; GR, gracilis; IQR, interquartile range; MRI, magnetic resonance imaging; PER, peroneus; RF, rectus femoris; SAR, sartorius; ST, semitendinosus; SM, semimembranosus; SOL, soleus; TA, tibialis anterior; TP, tibialis posterior; VI, vastus intermedius; VL, vastus lateralis; VM, vastus medialis

To visualize the separate effects of *age*, L_f and *PCSA* on the *logFF* (Table 2) on the original *FF* scale, we fitted the predicted FF based on the three individual predictors, while keeping the other two predictors at the median value. This resulted in the six graphs in Figure 3. For example, the top two panels represent the effect of *age* (x-axis) on *FF* (y-axis) for a muscle with a median L_f and *PCSA*. The graphs show an association for DMD of *FF* with *age* and L_f, but not with *PCSA* , whereas, for BMD, *FF* was associated with all three predictors.

Table 2. Output linear mixed effects model

DMD	**b-value** [a.u.]*	**SE b** [a.u.]*	**95% CI** [a.u.][a]	**P-value**[b]
Age [years]	0.281	0.055	0.167 - 0.394	**<0.001**
L_f [cm]	0.052	0.018	0.007 - 0.097	**0.030**
PCSA [cm^2]	0.011	0.008	-0.010 - 0.033	0.151
L_f **x *PCSA*** [a.u.]	0.003	0.001	0.000 - 0.006	**0.034**
BMD	**b-value** [a.u.]*	**SE b** [a.u.]*	**95% CI** [a.u.][a]	**P-value**[b]
Age [years]	0.031	0.015	0.013 - 1.250	**0.049**
L_f [cm]	0.114	0.027	1.130 - 3.437	**0.002**
PCSA [cm^2]	0.052	0.012	0.526 - 1.540	**0.002**
L_f **x *PCSA*** [a.u.]	0.007	0.002	1.426 - 4.432	**0.002**

Abbreviations: CI, confidence interval; L_f, fiber length; PCSA, physiological cross-sectional area ; SE, standard error
[a] *These values are represented in the Log odds transformed scale and correspond to the mean-centered predictors.*
[b] *These values are adjusted using the Holm-Bonferroni method*

In Figure 4, the interaction effect L_f *x PCSA* is illustrated. To this end, the *FF* was predicted for every combination of L_f and *PCSA* for a patient with a median *age*. The graphs show that the interaction effect is stronger in BMD than in DMD, indicated by the stronger curvature of the contours. In the DMD graph, the contours switch "direction" in the lower L_f regions, where a larger *PCSA* leads to lower *FF* values for L_f <7 cm and higher *FF* values for L_f >7 cm. What also stands out is that the *FF* values are higher in BMD than DMD, which can be explained by a higher average *FF* for a patient with the median *age* in BMD compared with DMD.

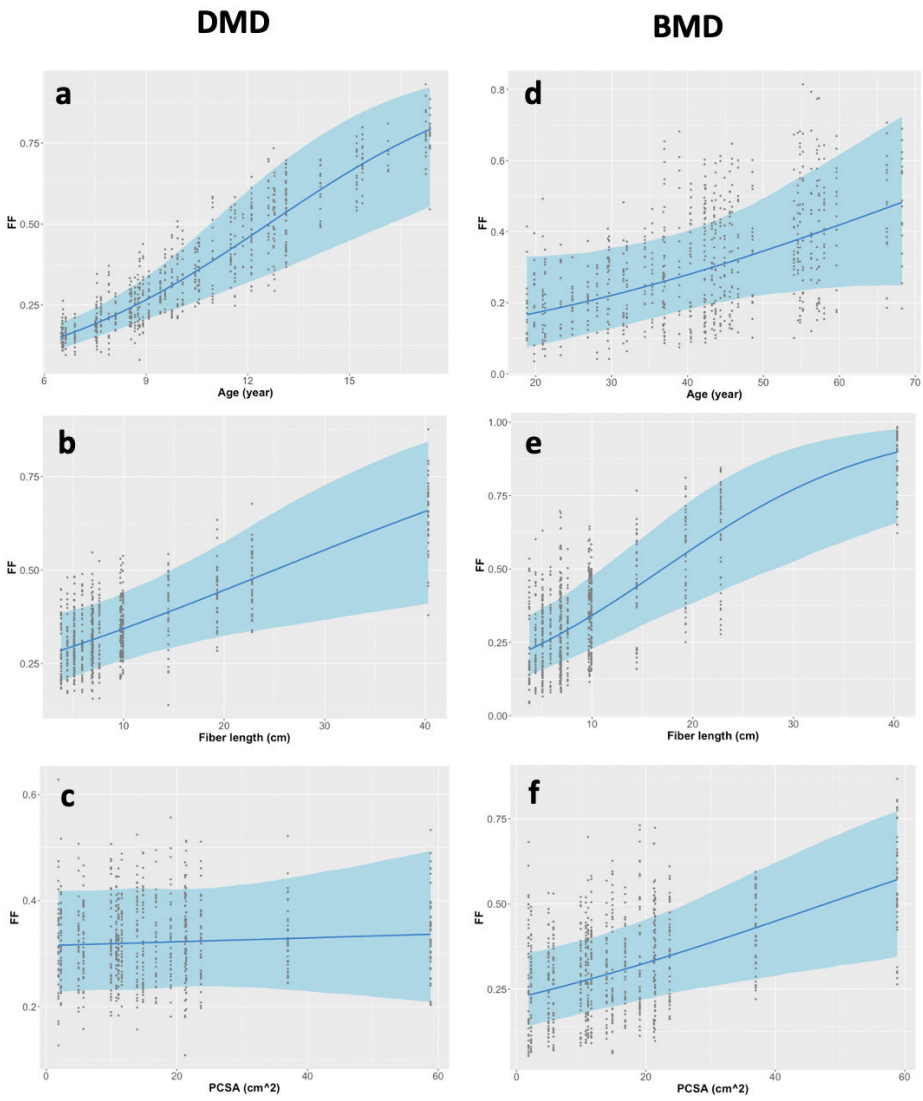

Figure 3: Prediction fits (blue line) for the three fixed effects and their effect on FF, while keeping the other two variables constant at the median value, with the 95% confidence intervals (blue bands) and the partial residuals for the 698 (DMD) and 731 (BMD) available data points (dots). The values are transformed back to the real FF scale. Abbreviations: BMD, Becker muscular dystrophy; DMD, Duchenne muscular dystrophy; FF, fat fraction; PCSA, physiological cross-sectional area

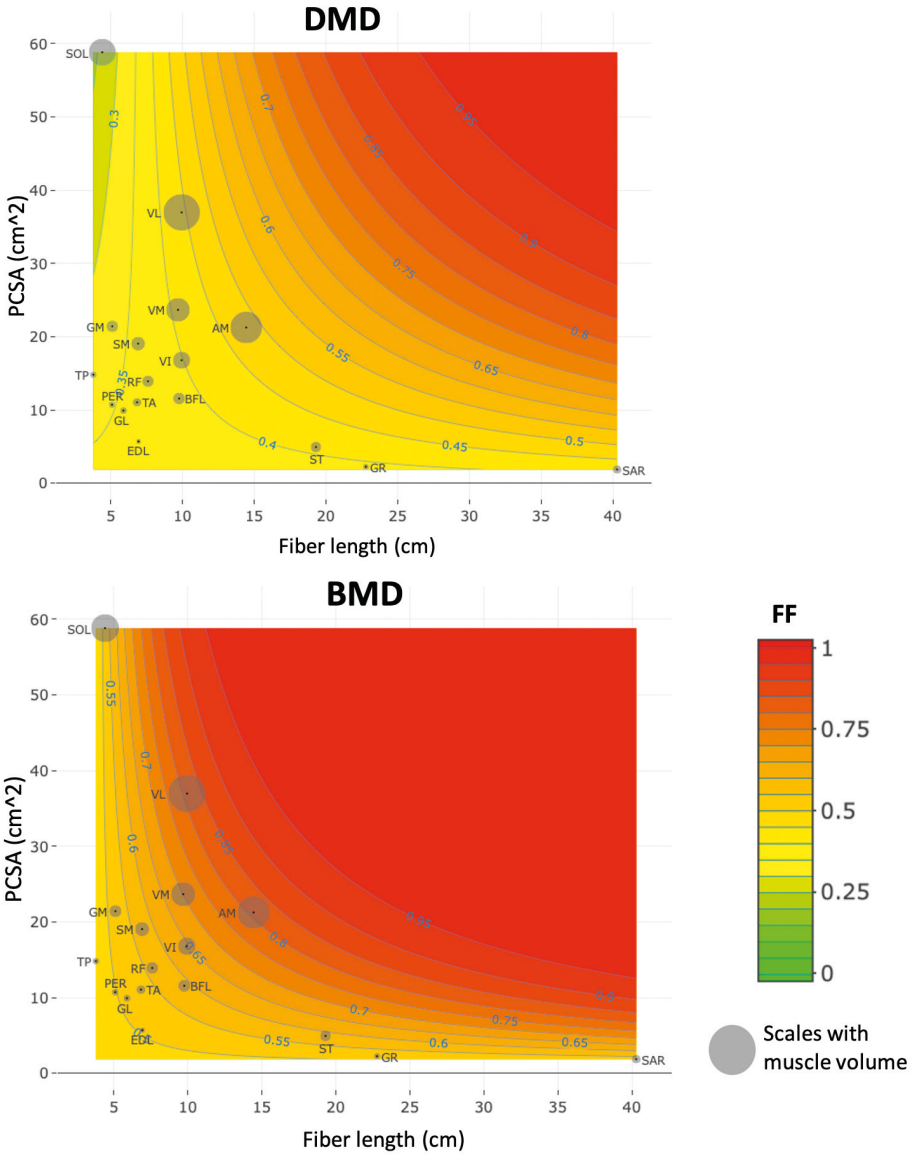

Figure 4: Visual representation of the interaction between fiber length and PCSA for DMD (left panel) and BMD (right panel). The color scale indicates the predicted FF for every combination of fiber length and PCSA for a patient with the median age (DMD≈10 years, BMD≈41 years). The contour lines are shown for every step of 0.05 FF. The muscles are located in the figure according to their fiber length and PCSA, the size of the circles is proportional to their mass as retrieved from Ward et al [22]. Abbreviations: BMD, Becker muscular dystrophy; DMD, Duchenne muscular dystrophy; FF, fat fraction; PCSA, physiological cross-sectional area

DISCUSSION

Our data are in line with our hypothesis: when correcting for age, muscles with long fibers and the interaction between fiber length and PCSA were associated with high fat fraction values in DMD and BMD. For BMD, a larger PCSA was significantly associated with a higher FF as well.

In the absence of dystrophin the inhomogeneity of force distribution within muscle fibers has been suggested to play a role in damage[10]. This hypothesis was corroborated with the observation that force propagation along the muscle fiber is slower in DMD patients[8]. Our results further support this hypothesis, as we have shown that muscles with long fibers are more susceptible to fat replacement in both DMD and BMD. Muscles with longer fibers are theoretically able to reach a high contraction velocity, and it is likely that an impaired force propagation in such fibers increases the inhomogeneity in force distribution, possibly leading to contraction-induced damage.

In BMD, muscles that are theoretically able to produce a high force (~large PCSA) also were associated with increased fat replacement. This could be due to the absence or dysfunction of dystrophin impairing force transmission to the sarcolemma[7]. The interaction effect between fiber length and PCSA may also be interpreted as representative of muscle volume, because muscle volume can be estimated by fiber length multiplied by PCSA. Muscle volume is proportional to the maximum muscle power, independent of the organization of these sarcomeres[9]. Thus, this interaction suggests that muscles with both long fibers and a large PCSA, and therefore can produce more power, are more susceptible to fat replacement. Because these muscles have a large volume, this is also in line with the clinical observation of a proximal-to-distal order of muscle degeneration[4].

The direction of the associations we found were comparable between DMD and BMD, but the effect of age was stronger in DMD than in BMD and the effect size of the significant parameters was larger in BMD (Table 2 and Figure 4). The smaller effect of age is likely due to the slower and more variable disease progression in BMD, as the age of onset and progression of muscle damage and clinical symptoms can vary greatly[29,30]. The larger effect size of the associations for fiber length and PCSA could be related to the slower progression of BMD compared to DMD[29,30]. In DMD, muscle damage likely starts soon after birth, and patients show muscle weakness early in life[31]. In BMD, symptom onset is usually much later, and extensive muscle damage only becomes apparent when patients are older, when the loads on muscles are higher. This could result in fat replacement being more influenced by muscle architecture in BMD patients.

Some limitations of the study should be acknowledged. First of all, we chose to include only fiber length and PCSA as characteristics determining the dynamic properties of a muscle, whereas muscle mass, pennation angle and fiber type composition also could play roles[9,32]. However, mass and pennation angle are highly dependent on fiber length and PCSA and would therefore add complexity to the model without significant additional information. Fiber type composition in human muscles, however, shows wide variation between individuals and heterogeneity within muscles[33,34]. Moreover, recent literature has described the existence of hybrid muscle fibers and question the classical idea of purely fast and slow fibers[35]. Therefore, reliable fiber type composition data sets including all leg muscle are not available. Second, we extracted the muscle characteristics from the study by Ward and colleagues[22] based on adult cadavers, whereas the DMD patients included in this study were on average 9.9 years old, ranging from 6.5 to 17.4 years at baseline. Therefore, the absolute values of the muscle characteristics may not be representative for the actual values of this cohort. However, proportions between body segments of children 8 years of age have been shown to be like to those of adults[36] and were therefore not expected to have a major impact on the associations found in this study. The average age of the BMD patients was 41 years old and the associations found in these patients were similar and even stronger than for the DMD patients. Therefore, it is possible that if we would have been able to include data on muscle characteristics of children, the associations would have been even stronger.

In this study we chose to include data of both DMD and BMD patients because they share the same pathological background, a mutation of the *DMD* gene. The fact that the resulting associations between muscle architecture and FF were comparable supports the hypothesis that muscle architecture indeed plays a role in the pathophysiology in these diseases. It would be of interest to perform the same analysis on other muscular dystrophies with affected proteins in other parts of the dystrophin-glycoprotein complex or with a completely different pathological background. In R9 dystroglycan-related limb-girdle muscular dystrophy, for example, a slightly different pattern of muscle involvement compared to DMD and BMD can be observed, although the affected protein is also part of the dystrophin-glycoprotein complex[37]. The pattern seems to show an earlier involvement of the short-fibered SM with larger PCSA and longer fibered ST with relatively small PCSA and a later involvement of the short-fibered RF with an average PCSA, when compared to DMD and BMD. Our mixed-effects model allows assessment of the role of muscle architecture, but inherently leaves part of the variance unexplained. Therefore, even with differences in muscle involvement, a role of muscle architecture should not be excluded. In addition, although proteins are part of the dystrophin-glycoprotein complex, they may have distinct roles; for example, it is known that the complex

plays an important role in multiple non-mechanical signaling pathways[38]. In a disease such as facioscapulohumeral muscular dystrophy[39–41] with a different pathophysiology, the mechanical interactions between the contractile proteins and the sarcolemma are intact[42] and structural and mechanical properties may be of less importance.

In conclusion, an association between muscle architecture and FF in DMD and BMD patients was observed. Muscles with longer muscle fibers were associated with higher FF values, and this effect was stronger if the PCSA of the muscle was larger. For BMD, a larger PCSA was also significantly associated with a higher FF. Our results indicate that larger muscles are more susceptible to fat replacement than small ones, confirming the clinical observation of a proximal-to-distal order of muscle degeneration. These results give more insight in the mechanical role in the pathophysiology of muscular dystrophies. Future longitudinal studies could explore the potential use of this information to track disease progression and responses to therapies.

STUDY FUNDING

This work was supported by the Netherlands Organization for Scientific Research (NWO), under research program VIDI, project number 917.164.90.

SUPPLEMENTAL MATERIAL

Supplemental Table 1 - an overview of mutations of DMD patients

DMD		
Participant ID	**Age at baseline [years]**	**Mutation**
1	12	Del 10
2	13	Del 53-54
3	11	Del 3-17
4	9	Del 46-52
5	13	Del 46-50
6	7	Exon 14: c.1609G>T p.(Gly537*)
7	11	Dup 49-50
8	7	Del 45
9	8	Del 45
10	9	Del 46-49
11	12	Del 8-32
12	8	Exon 19: c.2302C>T p.(Arg768*)
13	16	Del. Exon 48-52
14	6	Small deletion in exon 6: c.454_475del, p.(Pro152Serfs*11)
15	9	Del 3-7
16	9	Del 19-21
17	9	Del 8-9
18	11	Exon 66: c.9568C>T, p.(Arg3190*)
19	7	Del 50
20	13	Del 46-51
21	15	Del 3-7
22	6	Del 51

Supplemental Table 2 - an overview of mutations of BMD patients

BMD		
Participant ID	**Age at baseline [years]**	**Mutation**
23	57	Del 45-55
24	58	Exon 6: c.419T>A p.(Leu140His) VUS
25	55	Del 45-47
26	66	Del 45-55
27	47	Del 45-47
28	40	Del 3-4
29	37	Del 45-47
30	40	Del 45-47
31	43	Del 45-47
32	28	Dup 2-7
33	35	Del 45-47
34	30	Del 48-49
35	44	Del 45-47
36	55	Del 45-55
37	19	Del 45-47
38	25	Del 45-47
39	55	Dup 16-41
40	20	Del 3-7
41	44	Del 45-55
42	54	Del 45-48
43	42	Exon 29: c3940C>T p.(Arg1314*)
44	21	Del 30-44
45	32	Del 45-48
46	37	Exon 26: c.3515G>A p.(Trp1172*)

REFERENCES

1. Cros D, Harnden P, Pellissier JF, Serratrice G. Muscle hypertrophy in Duchenne muscular dystrophy - A pathological and morphometric study. Journal of Neurology 1989; 236:43–47.
2. Wokke BH, van den Bergen JC, Versluis MJ, Niks EH, Milles J, Webb AG, et al. Quantitative MRI and strength measurements in the assessment of muscle quality in Duchenne muscular dystrophy. Neuromuscular Disorders 2014; 24:409–416.
3. Tasca G, Iannaccone E, Monforte M, Masciullo M, Bianco F, Laschena F, et al. Muscle MRI in Becker muscular dystrophy. Neuromuscular Disorders 2012; 22:S100–S106.
4. Emery AEH. Muscular dystrophy into the new millennium. Neuromuscular Disorders 2002; 12:343–349. Published online: 2002. DOI: 10.1016/S0960-8966(01)00303-0.
5. Petrof BJ, Shrager JB, Stedman HH, Kelly AM, Sweeney HL. Dystrophin protects the sarcolemma from stresses developed during muscle contraction. Proceedings of the National Academy of Sciences 1993; 90:3710–3714.
6. Pasternak C, Wong S, Elson EL. Mechanical function of dystrophin in muscle cells. Journal of Cell Biology 1995; 128:355–361.
7. Rybakova IN, Patel JR, Ervasti JM. The dystrophin complex forms a mechanically strong link between the sarcolemma and costameric actin. Journal of Cell Biology 2000; 150:1209–1214.
8. Lacourpaille L, Hug F, Guével A, Péréon Y, Magot A, Hogrel J-Y, et al. New insights on contraction efficiency in patients with Duchenne muscular dystrophy. Journal of Applied Physiology 2014; 117:658–662.
9. Lieber RL. Skeletal muscle adaptability. I: Review of basic properties. Developmental Medicine & Child Neurology 1986; 28:390–397.
10. Claflin DR, Brooks S V. Direct observation of failing fibers in muscles of dystrophic mice provides mechanistic insight into muscular dystrophy. American journal of physiology. Cell physiology 2008; 294:C651–C658.
11. Ponrartana S, Ramos-Platt L, Wren TAL, Hu HH, Perkins TG, Chia JM, et al. Effectiveness of diffusion tensor imaging in assessing disease severity in Duchenne muscular dystrophy: preliminary study. Pediatric Radiology 2015; 45:582–589.
12. Gaeta M, Messina S, Mileto A, Vita GL, Ascenti G, Vinci S, et al. Muscle fat-fraction and mapping in Duchenne muscular dystrophy: Evaluation of disease distribution and correlation with clinical assessments preliminary experience. Skeletal Radiology 2012; 41:955–961.
13. Mankodi A, Bishop CA, Auh S, Newbould RD, Fischbeck KH, Janiczek RL. Quantifying disease activity in fatty-infiltrated skeletal muscle by IDEAL-CPMG in Duchenne muscular dystrophy. Neuromuscular Disorders 2016; 26:650–658.
14. Løkken N, Hedermann G, Thomsen C, Vissing J. Contractile properties are disrupted in Becker muscular dystrophy, but not in limb girdle type 2I. Annals of Neurology 2016; 80:466–471.
15. Hollingsworth KG, Higgins DM, McCallum M, Ward L, Coombs A, Straub V. Investigating the quantitative fidelity of prospectively undersampled chemical shift imaging in muscular dystrophy with compressed sensing and parallel imaging reconstruction. Magnetic Resonance in Medicine 2014; 72:1610–1619.
16. Hu X, Blemker SS. Musculoskeletal simulation can help explain selective muscle degeneration in Duchenne muscular dystrophy. Muscle and Nerve 2015; 52:174–182.

17. Naarding KJ, Reyngoudt H, van Zwet EW, Hooijmans MT, Tian C, Rybalsky I, et al. MRI vastus lateralis fat fraction predicts loss of ambulation in Duchenne muscular dystrophy. Neurology 2020; 94:e1386–e1394.
18. Hooijmans MT, Niks EH, Burakiewicz J, Anastasopoulos C, van den Berg SI, van Zwet E, et al. Non-uniform muscle fat replacement along the proximodistal axis in Duchenne muscular dystrophy. Neuromuscular Disorders 2017; 27:458–464.
19. Hooijmans MT, Froeling M, Koeks Z, Verschuuren JJGM, Webb A, Niks EH, et al. Multi-parametric MR in Becker muscular dystrophy patients. NMR in Biomedicine 2020; 33:1–15.
20. van den Bergen JC, Ginjaar HB, Van Essen AJ, Pangalila R, De Groot IJM, Wijkstra PJ, et al. Forty-five years of Duchenne muscular dystrophy in The Netherlands. Journal of Neuromuscular Diseases 2014; 1:99–109.
21. Wang X, Hernando D, Reeder SB. Sensitivity of chemical shift-encoded fat quantification to calibration of fat MR spectrum. Magnetic Resonance in Medicine 2016; 75:845–851.
22. Ward SR, Eng CM, Smallwood LH, Lieber RL. Are current measurements of lower extremity muscle architecture accurate? Clinical orthopaedics and related research 2009; 467:1074–1082.
23. Murphy RA, Beardsley AC. Mechanical properties of the cat soleus muscle in situ. American Journal of Physiology 1974; 227:1008–1013.
24. Bates D, Maechler M, Bolker B, Walker S. Fitting Linear Mixed-Effects Models Using lme4. Journal of Statistical Software 2015; 67:1–48.
25. Breheny P, Burchett W. Visualization of Regression Models Using visreg. The R Journal 2017; 9:56–71.
26. Rooney WD, Berlow YA, Triplett WT, Forbes SC, Willcocks RJ, Wang D-J, et al. Modeling disease trajectory in Duchenne muscular dystrophy. Neurology 2020; 94:e1622–e1633.
27. Kuznetsova A, Brockhoff PB, Christensen RHB. Package: Tests in Linear Mixed Effects Models. Journal of Statistical Software 2017; 82:1–26.
28. Holm S. A simple sequentially rejective multiple test procedure. Scandinavian journal of statistics 1979:65–70.
29. Angelini C, Fanin M, Pegoraro E, Freda MP, Cadaldini M, Martinello F. Clinical-molecular correlation in 104 mild X-linked muscular dystrophy patients: Characterization of sub-clinical phenotypes. Neuromuscular Disorders 1994; 4:349–358.
30. Comi GP, Prelle A, Bresolin N, Moggio M, Bardoni A, Gallanti A, et al. Clinical variability in becker muscular dystrophy genetic, biochemical and immunohistochemical correlates. Brain 1994; 117:1–14.
31. Arora H, Willcocks RJ, Lott DJ, Harrington AT, Senesac CR, Zilke KL, et al. Longitudinal timed function tests in duchenne muscular dystrophy: Imagingdmd cohort natural history. Muscle and Nerve 2018; 58:631–638.
32. Sacks RD, Roy RR. Architecture of the hind limb muscles of cats: Functional significance. Journal of Morphology 1982; 173:185–195.
33. Nygaard E, Sanchez J. Intramuscular variation of fiber types in the brachial biceps and the lateral vastus muscles of elderly men: How representative is a small biopsy sample? The Anatomical Record 1982; 203:451–459.
34. Simoneau J, Bouchard C. Genetic determinism of fiber type proportion in human skeletal muscle. The FASEB Journal 1995; 9:1091–1095.

35. Raz Y, van den Akker EB, Roest T, Riaz M, van de Rest O, Suchiman HED, et al. A data-driven methodology reveals novel myofiber clusters in older human muscles. FASEB Journal 2020; 34:5525–5537.
36. Burdi AR, Huelke DF, Snyder RG, Lowrey GH. Infants and children in the adult world of automobile safety design: Pediatric and anatomical considerations for design of child restraints. Journal of Biomechanics 1969; 2:267–280.
37. Willis TA, Hollingsworth KG, Coombs A, Sveen ML, Andersen S, Stojkovic T, et al. Quantitative Muscle MRI as an Assessment Tool for Monitoring Disease Progression in LGMD2I: A Multicentre Longitudinal Study. PLoS ONE 2013; 8:e70993.
38. Nichols B, Takeda S, Yokota T. Nonmechanical roles of dystrophin and associated proteins in exercise, neuromuscular junctions, and brains. Brain Sciences 2015; 5:275–298.
39. Andersen G, Dahlqvist JR, Vissing CR, Heje K, Thomsen C, Vissing J. MRI as outcome measure in facioscapulohumeral muscular dystrophy: 1-year follow-up of 45 patients. Journal of Neurology 2017; 264:438–447.
40. Gerevini S, Scarlato M, Maggi L, Cava M, Caliendo G, Pasanisi B, et al. Muscle MRI findings in facioscapulohumeral muscular dystrophy. European Radiology 2016; 26:693–705.
41. Fatehi F, Salort-Campana E, Le Troter A, Lareau-Trudel E, Bydder M, Fouré A, et al. Long-term follow-up of MRI changes in thigh muscles of patients with Facioscapulohumeral dystrophy: A quantitative study. PLoS ONE 2017; 12:e0183825.
42. Statland J, Tawil R. Facioscapulohumeral muscular dystrophy. Neurologic Clinics 2014; 22:1916–1931.